AGU PUBLICATIONS

Geophysical Research Letters

RESEARCH LETTER

10.1002/2015GL065152

Key Points:

- The libration amplitude, rotation rate, and pole orientation of Mercury have been measured
- The non-resonant rotation rate is interpreted in terms of a long-period libration
- Implications for Mercury's moment of inertia and interior structure are discussed

Supporting Information:

- Supporting Information S1
- Figure S1
- Figure S2

Correspondence to:
A. Stark,
alexander.stark@dlr.de

Citation:
Stark, A., J. Oberst, F. Preusker, S. J. Peale, J.-L. Margot, R. J. Phillips, G. A. Neumann, D. E. Smith, M. T. Zuber, and S. C. Solomon (2015), First MESSENGER orbital observations of Mercury's librations, *Geophys. Res. Lett.*, *42*, doi:10.1002/2015GL065152.

Received 29 JUN 2015
Accepted 11 AUG 2015
Accepted article online 9 SEP 2015

First MESSENGER orbital observations of Mercury's librations

Alexander Stark[1,2], Jürgen Oberst[1,3], Frank Preusker[1], Stanton J. Peale[4,5], Jean-Luc Margot[6,7], Roger J. Phillips[8], Gregory A. Neumann[9], David E. Smith[10], Maria T. Zuber[10], and Sean C. Solomon[11,12]

[1]German Aerospace Center, Institute of Planetary Research, Berlin, Germany, [2]Chair of Geodesy and Geoinformation Science, Technische Universität Berlin, Berlin, Germany, [3]Moscow State University for Geodesy and Cartography, Moscow, Russia, [4]Department of Physics, University of California, Santa Barbara, California, USA, [5]Deceased 14 May 2015, [6]Department of Earth, Planetary, and Space Sciences, University of California, Los Angeles, California, USA, [7]Department of Physics and Astronomy, University of California, Los Angeles, California, USA, [8]Southwest Research Institute, Boulder, Colorado, USA, [9]NASA Goddard Space Flight Center, Greenbelt, Maryland, USA, [10]Department of Earth, Atmospheric and Planetary Sciences, Massachusetts Institute of Technology, Cambridge, Massachusetts, USA, [11]Lamont-Doherty Earth Observatory, Columbia University, Palisades, New York, USA, [12]Department of Terrestrial Magnetism, Carnegie Institution of Washington, Washington, District of Columbia, USA

Abstract We have coregistered laser altimeter profiles from 3 years of MErcury Surface, Space ENvironment, GEochemistry, and Ranging (MESSENGER) orbital observations with stereo digital terrain models to infer the rotation parameters for the planet Mercury. In particular, we provide the first observations of Mercury's librations from orbit. We have also confirmed available estimates for the orientation of the spin axis and the mean rotation rate of the planet. We find a large libration amplitude of 38.9 ± 1.3 arc sec and an obliquity of the spin axis of 2.029 ± 0.085 arc min, results confirming that Mercury possesses a liquid outer core. The mean rotation rate is observed to be $(6.13851804 \pm 9.4 \times 10^{-7})$°/d (a spin period of 58.6460768 days ± 0.78 s), significantly higher than the expected resonant rotation rate. As a possible explanation we suggest that Mercury is undergoing long-period librational motion, related to planetary perturbations of its orbit.

1. Introduction

Mercury, moving deep in the gravitational field of the Sun, exhibits a distinctive rotation state. Its rotation is locked in a 3:2 spin-orbit resonance. Both the spin axis and the orbit plane normal precess around the instantaneous Laplace plane normal with a period near 330,000 years. In addition, action of the tidal torque of the Sun on the asymmetric mass distribution of the planet forces a physical libration in longitude, i.e., a small oscillation about the mean rotation. Measurement of the rotational state of Mercury, in combination with gravity field data, allows a determination of the size and state of Mercury's core [*Peale*, 1972, 1988; *Margot et al*., 2007, 2012; *Rivoldini et al*., 2009; *Smith et al*., 2012; *Hauck et al*., 2013; *Rivoldini and Van Hoolst*, 2013; *Dumberry and Rivoldini*, 2015].

The first accurate observations of Mercury's rotation [*Pettengill and Dyce*, 1965] demonstrated the distinctive resonance of the planet. On the basis of Mariner 10 images, the rotation period was constrained to 58.6461 ± 0.005 days [*Klaasen*, 1976]. More recently, Earth-based radar measurements of Mercury's obliquity and the amplitude of its forced libration [*Margot et al*., 2007] indicated that Mercury possesses a liquid core that is decoupled from the mantle on the 88 day timescale of the librations. However, the implications for the interior of Mercury from those radar observations were limited by uncertainties in the long-wavelength gravity field of the planet derived from Mariner 10 tracking observations. After the insertion of the MErcury Surface, Space ENvironment, GEochemistry, and Ranging (MESSENGER) spacecraft into orbit about Mercury in 2011, spacecraft Doppler and ranging measurements yielded precise estimates of Mercury's gravity field, particularly the coefficients of the terms of low degree and order in a spherical harmonic expansion of that field [*Mazarico et al*., 2014].

In this paper, we make use of orbital image and laser altimeter data acquired by MESSENGER to take a fresh look at the rotational state of Mercury. In particular, we report on the first determination of Mercury's librations from orbital observations. Our results validate those from Earth-based radar measurements by *Margot et al*. [2012]. We also update Mercury's spin axis orientation and rotation rate parameters. The

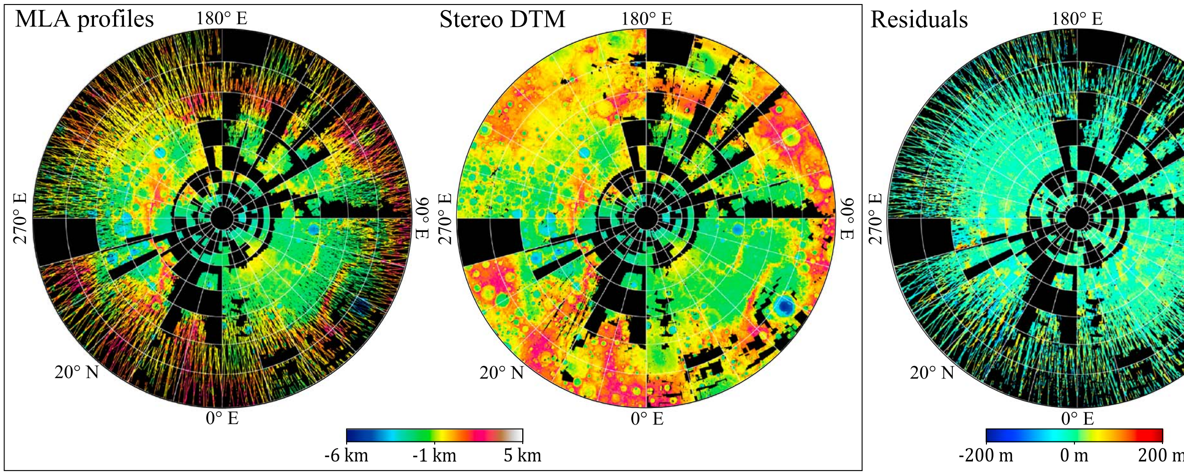

Figure 1. (left) MLA profiles used for measurement of rotational parameters. (middle) DTM tiles derived from stereo images by stereo photogrammetry. Each element of the grid corresponds to one DTM tile, for which separate offset and shift parameters are calculated. Gaps indicate lack of coverage by stereo DTMs. (right) Height residuals between MLA profiles and the stereo DTM tiles after coregistration. The mean value of the residuals is −1.2 m, and the standard deviation is 51.6 m. All maps are in stereographic projection centered at the north pole.

estimation of Mercury's obliquity and libration amplitude is performed using a novel approach [*Stark et al*., 2015a] by which we coregister laser altimeter profiles acquired over the 3 years of MESSENGER orbital operations to large-area topographic models derived from images by stereo photogrammetry.

2. Data Preparation

The Mercury Dual Imaging System (MDIS) [*Hawkins et al*., 2007] acquired more than 200,000 images during 3 years of observations, providing multiple coverage for nearly the entire surface at high resolution (better than 250 m/pixel). In contrast, data from the Mercury Laser Altimeter (MLA) [*Cavanaugh et al*., 2007] are largely confined to the northern hemisphere, as a result of limits on ranging distance and MESSENGER's highly eccentric, near-polar orbit.

We computed digital terrain models (DTMs) from stereo images following established procedures [*Gwinner et al*., 2010; *Preusker et al*., 2011; *Oberst et al*., 2014] that included image correlation and least squares block adjustment techniques. We combined at least three overlapping images to overcome uncertainties in spacecraft orbit, camera pointing direction, and calibration parameters, and consequently we obtained terrain models with very high internal robustness. Despite that geometric consistency, the stereo terrain models may have lateral and vertical offsets with respect to Mercury's center of mass. These global offsets are caused by residual uncertainties in spacecraft position and attitude (including camera pointing for individual images), as well as intrinsic camera calibration parameters. We produced 165 individual gridded DTMs (all at a grid size of 222 m/pixel) that cover approximately 50% of the northern hemisphere (Figure 1) with an average height error of 60 m. There are gaps in the image coverage because several geometric constraints (e.g., image resolution, incidence angle of sunlight, and stereo angle) must be satisfied in order to assemble stereo images. The topography in each DTM is expressed as height above a reference sphere of radius 2440 km.

The laser profiles acquired by the MLA instrument are highly complementary to the stereo DTMs. We used 3 years of MLA observations (29 March 2011 to 31 March 2014), including 2325 laser profiles across the northern hemisphere of Mercury (Figure 1). The highest density of data is in the north polar area, where the altimeter profiles converge. The nominal ranging accuracy is on the order of 1 m [*Cavanaugh et al*., 2007] and increases with ranging distance and off-nadir pointing. The profiles were obtained continuously, except for approximately 2 weeks in each Mercury orbit cycle. During those 2 weeks the spacecraft periapsis was over the dayside of Mercury, and the MLA was turned off to limit instrument temperature. At least two laser profiles per 24 h period (three profiles per day after the first year in orbit) were obtained, and observations covering more than 12 Mercury libration cycles (every ~88 days) and 18 Mercury rotation cycles (every ~59 days) are available for the analysis.

The comparison between laser altimeter observations acquired over a wide range of times and robust stereo DTMs with broad coverage and high spatial resolution is highly sensitive to rotational parameters for the planet.

3. Method

Our approach is to coregister the time-dependent spatially distributed network of laser altimeter profiles to the static topography of the stereo models. We compute the coordinates of the laser footprints in an inertial frame, i.e., the International Celestial Reference Frame (ICRF). The ICRF is approximately (to within 0.1 arc sec) the reference frame of the mean Earth equator and equinox of the J2000.0 epoch [*Archinal et al.*, 2011]. Coverage by laser profiles at a variety of rotation phases for Mercury allows us to determine all relevant parameters of the rotational model. We may thereby determine parameters that minimize height differences between laser altimeter measurements and the stereo DTMs. At the same time, we determine the static transformation parameters for each of the 165 DTMs, i.e., offsets, rotation angles, and scaling factors. We use a nonlinear least squares inversion to solve for the unknown parameters. Our observations are the radial height differences between the two data sets. The functional model $g(\mathbf{p})$ is given by

$$g(\mathbf{p}) = r_{\mathrm{DTM}}(\lambda(\mathbf{p}), \phi(\mathbf{p})) - |\boldsymbol{r}_{\mathrm{MLA}}(\mathbf{p})|, \tag{1}$$

where $r_{\mathrm{DTM}}(\lambda(\mathbf{p}), \phi(\mathbf{p}))$ is the height of the stereo DTM at the body-fixed latitude λ and longitude ϕ of the laser footprint and $|\boldsymbol{r}_{\mathrm{MLA}}(\mathbf{p})|$ is the height of the corresponding laser footprint (see *Stark et al.* [2015a] for more details). The parameter vector $\mathbf{p}$ includes the set of rotation parameters and the DTM transformation parameters for each of the available 165 DTM tiles. In total, 1161 parameters are determined from the coregistration.

The unknowns in the rotational model include the orientation of the rotational axis with respect to the ICRF, the rotation rate, and the amplitude of the forced libration at an 88 day period. In addition, we introduce two parameters to correct the coordinates of Mercury's center of mass within the planet's equatorial plane, a step needed because of small uncertainties in the ephemeris of Mercury.

For practical reasons the reference epoch for the rotational parameters is set to a midterm point of the MESSENGER orbital mission phase at MJD56353.5, or 2 March 2013, 12:00:00 barycentric dynamical time (TDB), 4809 days after the J2000.0 epoch. The precession of Mercury's spin axis, not resolvable within the duration of the MESSENGER orbital mission phase, is held fixed at $\alpha_1 = -0.032808$°/century and $\delta_1 = -0.0048464$°/century for the right ascension and declination of the spin axis, respectively [*Margot*, 2009; *Stark et al.*, 2015b]. Because Mercury is in a Cassini state [*Peale*, 1969], the spin axis is fixed in the orbit frame of reference and precesses at the same rate as the orbit. The precession of the spin axis is important, as during the 3 years of MESSENGER observations considered here the spin axis precessed by 1.8 arc sec. Given the precession rates, the spin axis orientation at the J2000.0 epoch can be calculated for comparison.

We adopt a model for the annual longitudinal librations φ_{lib}, which follows from the solution of the differential equation for tidal torque [*Goldreich and Peale*, 1966; *Margot et al.*, 2007, 2009]

$$\varphi_{\mathrm{lib}}(t) = \sum\nolimits_k g_{88/k} \sin(k n_0 (t + t_0)), \tag{2}$$

where $n_0 = 4.09233445$°/d is the mean motion of Mercury, $t_0 = (4809 + 42.71182)$ days defines the libration phase at the reference epoch, and $g_{88/k}$ denotes the amplitude of the kth harmonic of the libration. The amplitudes follow a recursive relation

$$g_{88/(k+1)} = g_{88/k} \frac{G_{2\,0\,1}(k+1, e)}{G_{2\,0\,1}(k, e)}, \tag{3}$$

where $G_{2\ 0\ 1}(k, e) = [G_{2\ 0\ 1-k}(e) - G_{2\ 0\ 1+k}(e)]/k^2$ and $G_{2\ 0\ 1\pm k}(e)$ are Kaula's eccentricity functions [*Kaula*, 2000] and $e = 0.2056317$ is the orbital eccentricity of Mercury [*Stark et al.*, 2015b]. We limit the libration model to five harmonics, as we observed that the amplitudes of the higher-frequency terms (on the order of $0.0001 g_{88}$) are negligible.

In addition to the annual libration, there could be long-period librations with periods of several years, resulting from periodic perturbations to Mercury's orbit by other planets or other mechanisms (see below). Although planetary perturbations to Mercury's orbit are relatively small, their effect can be enhanced when their frequency is close to the free libration frequency of Mercury. However, considering the limited observational period of about 3 years, we are unable to track these long-period librations. Instead, we have searched for small deviations of Mercury's spin rate from the resonant spin rate.

Other entries in the parameter vector **p** describe adjustments to the DTM tiles, which include three rotation angles, three components of a translation vector, and a scaling factor [*Stark et al*., 2015a] for each DTM tile. The static transformations allow for the coregistration of the data sets in the spatial domain, whereas the adjustment of the rotational parameters ensures a proper alignment of the laser altimetry footprints at their observation time. Note that because the small DTM tiles include regional topography, the similarity transformation can be nonunique, but with the inclusion of all seven transformation parameters, we allow maximal flexibility in the spatial coregistration. Because of the gaps in the stereo coverage mentioned above, only 50% of the full set of MLA measurements can be used in the estimation process. To obtain subpixel heights of the gridded DTMs at the coordinates of the laser footprints, we perform a bilinear interpolation of the DTM heights, whereby an area of 3×3 pixels is approximated by an inclined plane. This step is not a limitation given that the "effective resolution" of the DTMs was determined to be as large as 3.8 km [*Stark et al*., 2015a].

In contrast to the stereo DTM data, which are coarse but fairly uniform in height precision, the MLA data, although more precise, suffer from individual uncertainties introduced by variations in ranging distance and occasional off-nadir pointing. We therefore introduced a weighting scheme for each individual observation (see *Stark et al*. [2015a]). In addition, we introduced a threshold to identify and remove extreme outliers (such as false detected laser pulses, or small-scale topographic features not seen in the stereo DTM); the threshold is estimated from the standard deviation of the residuals from the preceding iteration step.

We initiated the iterations with the rotational axis aligned with the orbit normal, the rotation rate set precisely to the resonant rotation rate of 6.138506839 °/d, and the libration amplitude set to zero. The DTM transformation parameters were initialized under the assumption of perfect alignment of DTMs and MLA data.

Although the parameter estimation procedure yields formal uncertainties from the covariance matrix, we also derive more robust uncertainty estimations. We performed 100 Monte Carlo simulations of artificial MLA observations over the complete time span of 3 years treated here, and we derived uncertainties in the unknowns from their distribution in the simulation results. To account for the different resolution of the data sets, we performed a synthesis of artificial laser altimeter measurements derived from the topography of the stereo DTMs. Each simulation was performed as follows. We started with the inertial spacecraft coordinates immediately before the transmission of the laser pulse. With the nominal information on spacecraft position and attitude, as well as laser pulse time of flight, we obtained the height information from the DTM at the laser footprint coordinates. Then, we added random errors to the nominal spacecraft position and attitude and generated high-resolution topography from the DTM heights at the nominal laser footprint locations. Thus, we obtained synthetic laser altimeter topography at perturbed laser footprint locations. The simulated observables were then coregistered and led to slightly different best fit parameters. More details on the simulation of topographic observables have been given by *Stark et al*. [2015a]. The covariance of the unknown parameters $\boldsymbol{C}_\mathrm{p}^*$ is finally given by

$$\left[\boldsymbol{C}_\mathrm{p}^*\right]_{ij} = \frac{1}{99}\sum\nolimits_{k=1}^{100}\left(p_i^k - p_i^*\right)\left(p_j^k - p_j^*\right), \tag{4}$$

where p_i^* and p_i^k denote the ith best fit parameters from the actual data and from the kth simulation of observations, respectively. The covariance matrix $\boldsymbol{C}_p^*$ is used to calculate uncertainties for all derived quantities, such as the moment of inertia values presented below.

4. Results

Following the inversion, we obtained a parameter set for the rotational model of Mercury (Table 1). We performed 15 iterations, and stopped the calculation when the improvement in the root-mean-

Table 1. Rotational Parameters (Observed) and Corresponding Interior Structural Parameters (Derived) for Mercury[a]

Quantity	Value
Observed Rotational Parameters	
Annual libration amplitude	38.9 ± 1.3 arc sec
Mean rotation rate[b]	$(6.13851804 \pm 9.4 \times 10^{-7})$°/d
Mean rotation period[b]	58.6460768 ± 0.0000090 days
Right ascension of spin axis[c]	281.00980 ± 0.00088°
Declination of spin axis[c]	61.4156 ± 0.0016°
Obliquity of the spin axis	2.029 ± 0.085 arc min
Derived Interior Structure Parameters[d]	
$(B - A)/C_m$	$(2.206 \pm 0.074) \times 10^{-4}$
C/MR^2	0.346 ± 0.011
C_m/C	0.421 ± 0.021
C_m/MR^2	0.1458 ± 0.0049

[a]Gravitational parameters are from *Mazarico et al*. [2014].
[b]Mean value during the time between 29 March 2011 and 31 March 2014.
[c]At J2000.0 with respect to the ICRF.
[d]Under the assumption that there is no or at most a small solid inner core.

squared residual was less than the centimeter level. We determined an annual libration amplitude of g_{88} = 38.9 ± 1.3 arc sec, corresponding approximately to 460 ± 15 m at the equator. These values are in agreement with the results from Earth-based radar observations [*Margot et al*., 2012], cited as 38.5 ± 1.6 arc sec. The absolute difference between the two values is 0.4 arc sec, well within the respective one-standard-deviation errors. This high libration amplitude indicates that the rotation of Mercury's crust and mantle is decoupled from that of the fluid core (see below).

The mean rotation rate of Mercury was determined as $(6.13851804 \pm 9.4 \times 10^{-7})$°/d, higher by 14.72 arc sec per year (or ~2 ppm) than the expected resonant rate of 6.1385068°/d [*Stark et al*., 2015b]. The estimated rotation rate corresponds to a rotation period of 58.6460768 ± 0.0000090 days and is lower by 9.24 s than the resonant rotation period. The value obtained for the rotation rate is also significantly higher than the value of 6.1385025°/d currently adopted by the International Astronomical Union (IAU) [*Archinal et al*., 2011], but it is in agreement with the value estimated from Mariner 10 imaging of 6.13852 ± 0.00052°/d [*Klaasen*, 1976]. Recent estimates derived from the rotation of the gravity field of Mercury indicate a rotation rate of $(6.13851079 \pm 1.2 \times 10^{-6})$°/d [*Mazarico et al*., 2014], also greater than the IAU value and the resonant rotation value but not in agreement with our estimate.

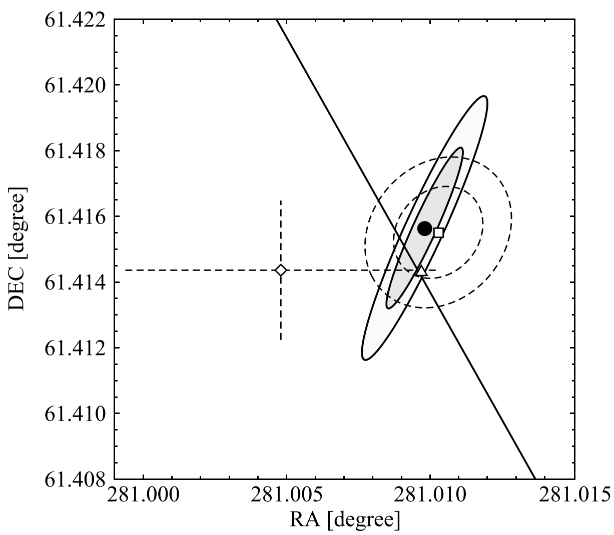

Figure 2. Right ascension (RA) and declination (DEC) of Mercury's spin axis in the ICRF (filled circle) and one- and two-standard-deviation uncertainties (shaded ellipses). The ground-based estimates of *Margot et al*. [2007] and *Margot et al*. [2012] are shown by the triangle and square, respectively; one- and two-standard-deviation errors are shown for the latter determination (dashed ellipses). The estimate inferred from the gravity field rotation [*Mazarico et al*., 2014] is denoted by a diamond, and the errors shown are at one standard deviation. The oblique line shows the predicted locations of Cassini state 1 from the values of *Stark et al*. [2015b], which are consistent with those of *Yseboodt and Margot* [2006]. All spin axis orientations correspond to the J2000.0 epoch.

At the reference epoch of MJD56353.5 the orientation of the spin axis of Mercury's mantle is obtained at α_0 (MJD56353.5) = 281.00548 ± 0.00088° in right ascension and δ_0 (MJD56353.5) = 61.4150 ± 0.0016° in declination with respect to the ICRF. With precession as discussed above, we find α_0 = 281.00980 ± 0.00088° and δ_0 = 61.4156 ± 0.0016° at the J2000.0 epoch (Figure 2). The obliquity of the spin axis with respect to the mean orbit normal $\left(\alpha_0^{OP} = 280.98797°;\ \delta_0^{OP} = 61.4478°\right)$ is 2.029 ± 0.085 arc min. We find that the spin axis orientation is slightly offset by 1.7 arc sec, but well within the error bounds, from the precise Cassini state 1 position, known to within 0.3 arc sec [*Stark et al.*, 2015b]. Again, all data are in excellent agreement with Earth-based radar results [*Margot et al*., 2007, 2012] (Figure 2). The absolute angular deviation from the most recent Earth-based result [*Margot et al*., 2012] is only 1 arc sec. We observe somewhat larger values for the right ascension and declination of the spin axis than the gravity-based estimates of *Mazarico et al*. [2014]. However, given the large error in the gravity-based estimate, further discussion of this difference in spin axis position is not warranted.

5. Implications and Discussion

The amplitude of the annual libration provides information on the coupling between the mantle and the core of the planet. For a molten outer core, the rotation of outer core and mantle will be nearly fully decoupled, and a large libration amplitude is possible. On the other hand, if the entire core is solid, the mantle and core will have a common rotation, in which case a smaller libration amplitude is expected. The observed large libration amplitude value of $g_{88} = 38.9 \pm 1.3$ arc sec suggests at most limited coupling between mantle and outer core, and we can compute the corresponding asymmetry of the mass distribution within the planet from [*Peale*, 1972; *Dumberry et al*., 2013; *Dumberry and Rivoldini*, 2015]

$$\frac{B-A}{C_\mathrm{m}} = \frac{2g_{88}}{3G_{2\,0\,1}(1,e)}(1+\xi), \tag{5}$$

where $A < B$ are the moments of inertia of the planet about the principal equatorial axes and C_m is the polar moment of inertia of the mantle and crust. The parameter ξ is a small correction that depends on the size of the solid inner core and interior density structure [*Veasey and Dumberry*, 2011; *Van Hoolst et al*., 2012; *Dumberry et al*., 2013; *Dumberry and Rivoldini*, 2015]. The correction factor in equation (5) is below the uncertainty in the libration amplitude g_{88} even for a large inner core with a radius of about 1500 km [*Van Hoolst et al*., 2012; *Dumberry et al*., 2013]. Hence, we assume that the equatorial asymmetry is due to the mantle alone, and we thereby neglect the coupling to a possible solid inner core, so $\xi \approx 0$. From our estimate of g_{88} we find a value of $(B-A)/C_\mathrm{m} = (2.206 \pm 0.074) \times 10^{-4}$. This value provides an important constraint on the interior structure of the planet.

One possible explanation for the observation of a greater rotation rate than the expected resonant rotation value is that the planet is undergoing forced long-period librations, which modulate the mean rotation rate on time-scales of several years [*Peale et al*., 2007; *Yseboodt et al*., 2010, 2013]. The amplitude of the long-period libration is strongly related to the free libration frequency ω_0 of the planet [*Yseboodt et al*., 2010; *Dumberry et al*., 2013]

$$\omega_0 = n_0\sqrt{3G_{2\,0\,1}(e)\frac{B-A}{C_\mathrm{m}}}, \tag{6}$$

where $G_{2\ 0\ 1}(e) = 7/2\ e + 123/16\ e^3 + O(e^5) \approx 0.654259$. A large inner core can significantly change the free libration frequency given in equation (6). Here we discuss the case where Mercury has no or only a small solid inner core. The observed value of the mass distribution asymmetry $(B-A)/C_\mathrm{m} = (2.206 \pm 0.074) \times 10^{-4}$ indicates that the free libration frequency of Mercury is 0.5428 ± 0.0091 radians per year, corresponding to a period of 11.58 ± 0.19 years, close to the period of the orbital perturbations of Mercury's orbit by Jupiter (11.864 years). With the analytical model of *Yseboodt et al*. [2010] and given a damping time of the free libration of about 2×10^5 years [*Peale*, 2005], we searched for the free libration frequency that would be consistent with the observed rotation rate. We find that such high deviations from the resonant rate are possible only when they are resonantly enhanced, i.e., when the free libration frequency of Mercury is close to the frequency of the orbital perturbation. Because of its proximity to Jupiter's orbital frequency, a free libration frequency of 0.536 radians per year (11.725 years) could lead to a sufficient enhancement of the effect of the small orbital perturbations of Mercury's orbit to be in agreement with the observed mean rotation rate. The libration frequency inferred from long-period libration considerations (see supporting information for more details) corresponds to a mass distribution asymmetry of $(B-A)/C_\mathrm{m} = 2.1498 \times 10^{-4}$. Note that this value is consistent with our estimate from the annual libration amplitude g_{88} and the estimate by *Margot et al.* [2012] to within the one standard deviation uncertainty. In addition to forced longitudinal librations, free librations with large amplitudes are also theoretically possible under the condition of small internal dissipation or recent excitation. This discussion, of course, was of only

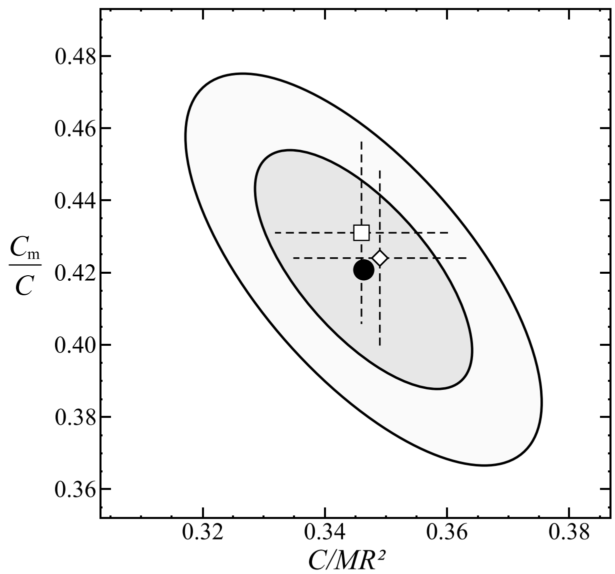

Figure 3. Mercury's normalized polar moment of inertia C/MR^2 and the fractional moment of inertia of the mantle and crust C_m/C as inferred from measured values for libration amplitude and obliquity (filled circle). The ellipses denote one- and two-standard-deviation uncertainties. The square and the diamond with dashed one-standard-deviation uncertainties show the estimates of *Margot et al*. [2012] and *Mazarico et al*. [2014], respectively.

one possible explanation for an increased rotation rate. Other mechanisms such as contributions from the solid inner core [*Dumberry*, 2011; *Van Hoolst et al*., 2012; *Dumberry et al*., 2013; *Yseboodt et al*., 2013] or turbulent convection in the fluid core [*Koning and Dumberry*, 2013] can also affect the rotation rate.

Peale et al. [2014] considered several coupling mechanisms between the core and the mantle, any of which could lead to a mantle spin orientation that lags the precise Cassini state 1. Further, the small offset from the precise Cassini state 1 may represent the signature of a free precession. Nonetheless, the parameters of Cassini state 1 fall within the uncertainties in our estimate of the spin axis orientation. Further work is needed to understand the interplay of different torques acting on the mantle and the core, as well as the Cassini state 1 position, which is here based on the theory for a completely solid planet.

From the observed obliquity of 2.029 ± 0.085 arc min we can compute the normalized polar moment of inertia of the planet C/MR^2, where M is the mass of the planet and R its mean radius. We use equation (4) of *Peale* [1981] and $\mu \sin \iota = 2.8645 \times 10^{-6}$/year and $\mu \cos \iota = 18.9 \times 10^{-6}$/year [*Stark et al*., 2015b], where μ is the precession rate of the mean orbital plane and ι is the angle between the orbital plane and the Laplace plane. Further, we use the most recent estimates for the gravitational coefficients $J_2 = (5.03216 \pm 0.00093) \times 10^{-6}$ and $C_{22} = (0.80389 \pm 0.00019) \times 10^{-6}$ [*Mazarico et al*., 2014]. We obtain a polar moment of inertia of the planet of $C/MR^2 = 0.346 \pm 0.011$.

From the identity relation [*Peale*, 1972; *Margot et al*., 2012]

$$\frac{C_m}{C} = 4C_{22}\frac{MR^2}{C}\frac{C_m}{B-A}, \tag{7}$$

and our value for C/MR^2 and $(B-A)/C_m$, we can compute the ratio C_m/C between the polar moment of inertia of the outer rigid shell C_m and that of the entire planet C. We find a value $C_m/C = 0.421 \pm 0.021$ and consequently $C_m/MR^2 = 0.1458 \pm 0.0049$ (Figure 3). The covariance between C/MR^2 and C_m/C is -8.04×10^{-5} (Figure 3). These results are again in very good agreement with those derived from Earth-based estimates of obliquity and libration amplitude by *Margot et al*. [2012] and the gravity field of *Mazarico et al*. [2014].

The derived values for the moment of inertia form first-order constraints for the interior structure of Mercury. Given the total mass and shape of Mercury [*Perry et al*., 2015], one can constrain the densities of the core and the mantle, as well as the location of the core-mantle boundary. Models for the interior structure of Mercury treat distinct crustal and mantle layers, the possibility of compositional layering in the mantle, the ellipticity of layer boundaries, and the effects of a possible solid inner core [*Smith et al*., 2012; *Hauck et al*., 2013; *Rivoldini and Van Hoolst*, 2013; *Dumberry and Rivoldini*, 2015]. The tidal Love number k_2, recently determined from MESSENGER's radio science data [*Mazarico et al*., 2014], can provide an additional constraint on the structure and rheology of the planetary interior [*Padovan et al*., 2014].

For our analysis we used only 3 years of MLA observations and a small fraction of processed images. Expanding the data sets and elaborating the coregistration method [*Stark et al*., 2015a] by the use of crossover points on laser profiles are warranted in future applications of the methods applied here. Use of crossovers may provide additional constraints, which could further reduce the uncertainties in the rotational parameters. Our estimates of the uncertainties in the rotational parameters are based on a pessimistic scenario with a relatively poor knowledge of the position and attitude of the spacecraft and its alignment to MLA. Nonetheless, because of the combination of data from varying observation conditions in our analysis, e.g., variations in the distance of MESSENGER to Mercury's surface from 200 km to 1790 km, we expect that the estimation of rotational parameters presented here is robust.

6. Conclusion

With laser altimetry and imaging data from the MESSENGER spacecraft we provide the first orbital measurement of the amplitude of the annual libration of Mercury. Further, we obtain values for the mean rotation rate and the orientation of the spin axis. The results are in excellent agreement with existing estimates from ground-based radar observations [*Margot et al.*, 2007, 2012] and measurements of the rotation of the gravity field [*Mazarico et al.*, 2014]. Considering that the MESSENGER spacecraft operated for more than an additional year beyond the data treated in this paper, further refinement of Mercury's rotational parameters can be expected from future analysis with the full set of orbital observations.

Acknowledgments

This research was funded by a grant from the German Research Foundation (OB124/11-1). J. Oberst gratefully acknowledges being hosted by MIIGAiK and supported by the Russian Science Foundation under project 14-22-00197. The MESSENGER mission is supported by the NASA Discovery Program under contract NAS5-97271 to The Johns Hopkins University Applied Physics Laboratory and NASW-00002 to the Carnegie Institution of Washington. We acknowledge the contributions of the MESSENGER spacecraft team and MLA and MDIS instrument teams in acquiring the observations used herein. MESSENGER data are available from the Planetary Data System (https://pds.jpl.nasa.gov). We thank Hauke Hussmann and Marie Yseboodt for their helpful comments and discussions. Reviews by Mathieu Dumberry and an anonymous reviewer substantially improved this paper.

The Editor thanks Mathieu Dumberry and an anonymous reviewer for their assistance in evaluating this paper.

References

Archinal, B. A., et al. (2011), IAU Working Group on Cartographic Coordinates and Rotational Elements: 2009, *Celestial Mech. Dyn. Astron.*, *109*, 101–135, doi:10.1007/s10569-010-9320-4.

Cavanaugh, J. F., et al. (2007), The Mercury Laser Altimeter instrument for the MESSENGER mission, *Space Sci. Rev.*, *131*, 451–479, doi:10.1007/s11214-007-9273-4.

Dumberry, M. (2011), The free librations of Mercury and the size of its inner core, *Geophys. Res. Lett.*, *38*, L16202, doi:10.1029/2011GL048277.

Dumberry, M., and A. Rivoldini (2015), Mercury's inner core size and core-crystallization regime, *Icarus*, *248*, 254–268, doi:10.1016/j.icarus.2014.10.038.

Dumberry, M., A. Rivoldini, T. Van Hoolst, and M. Yseboodt (2013), The role of Mercury's core density structure on its longitudinal librations, *Icarus*, *225*, 62–74, doi:10.1016/j.icarus.2013.03.001.

Goldreich, P., and S. J. Peale (1966), Spin-orbit coupling in the solar system, *Astron. J.*, *71*, 425–438, doi:10.1086/109947.

Gwinner, K., F. Scholten, F. Preusker, S. Elgner, T. Roatsch, M. Spiegel, R. Schmidt, J. Oberst, R. Jaumann, and C. Heipke (2010), Topography of Mars from global mapping by HRSC high-resolution digital terrain models and orthoimages: Characteristics and performance, *Earth Planet. Sci. Lett.*, *294*, 506–519, doi:10.1016/j.epsl.2009.11.007.

Hauck, S. A., II, et al. (2013), The curious case of Mercury's internal structure, *J. Geophys. Res. Planets*, *118*, 1204–1220, doi:10.1002/jgre.20091.

Hawkins, S. E., III, et al. (2007), The Mercury Dual Imaging System on the MESSENGER spacecraft, *Space Sci. Rev.*, *131*, 247–338, doi:10.1007/s11214-007-9266-3.

Kaula, W. M. (2000), *Theory of Satellite Geodesy: Applications of Satellites to Geodesy*, 160 pp., Dover, Mineola, N. Y.

Klaasen, K. P. (1976), Mercury's rotation axis and period, *Icarus*, *28*, 469–478, doi:10.1016/0019-1035(76)90120-2.

Koning, A., and M. Dumberry (2013), The free librations of Mercury and the size of its inner core, *Icarus*, *223*, 40–47, doi:10.1016/j.icarus.2012.11.022.

Margot, J. L. (2009), A Mercury orientation model including non-zero obliquity and librations, *Celestial Mech. Dyn. Astron.*, *105*, 329–336, doi:10.1007/s10569-009-9234-1.

Margot, J. L., S. J. Peale, R. F. Jurgens, M. A. Slade, and I. V. Holin (2007), Large longitude libration of Mercury reveals a molten core, *Science*, *316*, 710–714, doi:10.1126/science.1140514.

Margot, J. L., S. J. Peale, S. C. Solomon, S. A. Hauck II, F. D. Ghigo, R. F. Jurgens, M. Yseboodt, J. D. Giorgini, S. Padovan, and D. B. Campbell (2012), Mercury's moment of inertia from spin and gravity data, *J. Geophys. Res.*, *117*, E00L09, doi:10.1029/2012JE004161.

Mazarico, E., A. Genova, S. Goossens, F. G. Lemoine, G. A. Neumann, M. T. Zuber, D. E. Smith, and S. C. Solomon (2014), The gravity field, orientation, and ephemeris of Mercury from MESSENGER observations after three years in orbit, *J. Geophys. Res. Planets*, *119*, 2417–2436, doi:10.1002/2014JE004675.

Oberst, J., K. Gwinner, and F. Preusker (2014), Exploration and analysis of planetary shape and topography using stereophotogrammetry, in *Encyclopedia of the Solar System*, edited by T. Spohn, D. Breuer, and T. V. Johnson, pp. 1223–1233, Elsevier, Boston, Mass.

Padovan, S., J. L. Margot, S. A. Hauck II, W. B. Moore, and S. C. Solomon (2014), The tides of Mercury and possible implications for its interior structure, *J. Geophys. Res. Planets*, *119*, 850–866, doi:10.1002/2013JE004459.

Peale, S. J. (1969), Generalized Cassini's laws, *Astron. J.*, *74*, 483–489, doi:10.1086/110825.

Peale, S. J. (1972), Determination of parameters related to the interior of Mercury, *Icarus*, *17*, 168–173, doi:10.1016/0019-1035(72)90052-8.

Peale, S. J. (1981), Measurement accuracies required for the determination of a Mercurian liquid core, *Icarus*, *48*, 143–145, doi:10.1016/0019-1035(81)90160-3.

Peale, S. J. (1988), The rotational dynamics of Mercury and the state of its core, in *Mercury*, edited by F. Vilas, C. R. Chapman, and M. S. Matthews, pp. 461–493, Univ. of Arizona Press, Tucson.

Peale, S. J. (2005), The free precession and libration of Mercury, *Icarus*, *178*, 4–18, doi:10.1016/j.icarus.2005.03.017.

Peale, S. J., M. Yseboodt, and J. L. Margot (2007), Long-period forcing of Mercury's libration in longitude, *Icarus*, *187*, 365–373, doi:10.1016/j.icarus.2006.10.028.

Peale, S. J., J. L. Margot, S. A. Hauck II, and S. C. Solomon (2014), Effect of core–mantle and tidal torques on Mercury's spin axis orientation, *Icarus*, *231*, 206–220, doi:10.1016/j.icarus.2013.12.007.

Perry, M. E., et al. (2015), The low-degree shape of Mercury, *Geophys. Res. Lett.*, *42*, doi:10.1002/2015GL065152.

Pettengill, G. H., and R. B. Dyce (1965), A radar determination of the rotation of the planet Mercury, *Nature*, *206*, 1240, doi:10.1038/2061240a0.

Preusker, F., J. Oberst, J. W. Head, T. R. Watters, M. S. Robinson, M. T. Zuber, and S. C. Solomon (2011), Stereo topographic models of Mercury after three MESSENGER flybys, *Planet. Space Sci.*, *59*, 1910–1917, doi:10.1016/j.pss.2011.07.005.

Rivoldini, A., and T. Van Hoolst (2013), The interior structure of Mercury constrained by the low-degree gravity field and the rotation of Mercury, *Earth Planet. Sci. Lett.*, *377–378*, 62–72.

Rivoldini, A., T. Van Hoolst, and O. Verhoeven (2009), The interior structure of Mercury and its core sulfur content, *Icarus*, *201*, 12–30, doi:10.1016/j.icarus.2008.12.020.

Smith, D. E., et al. (2012), Gravity field and internal structure of Mercury from MESSENGER, *Science*, *336*, 214–217, doi:10.1126/science.1218809.

Stark, A., J. Oberst, F. Preusker, K. Gwinner, S. J. Peale, J. L. Margot, R. J. Phillips, M. T. Zuber, and S. C. Solomon (2015a), Mercury's rotation parameters from MESSENGER image and laser altimetry data: A feasibility study, *Planet. Space Sci.*, doi:10.1016/j.pss.2015.05.006, in press.

Stark, A., J. Oberst, and H. Hussmann (2015b), Mercury's resonant rotation from secular orbital elements, *Celestial Mech. Dyn. Astron.*, doi:10.1007/s10569-015-9633-4, in press.

Van Hoolst, T., A. Rivoldini, R. M. Baland, and M. Yseboodt (2012), The effect of tides and an inner core on the forced longitudinal libration of Mercury, *Earth Planet. Sci. Lett.*, *333–334*, 83–90, doi:10.1016/j.epsl.2012.04.014.

Veasey, M., and M. Dumberry (2011), The influence of Mercury's inner core on its physical libration, *Icarus*, *214*, 265–274, doi:10.1016/j.icarus.2011.04.025.

Yseboodt, M., and J. L. Margot (2006), Evolution of Mercury's obliquity, *Icarus*, *181*, 327–337, doi:10.1016/j.icarus.2005.11.024.

Yseboodt, M., J. L. Margot, and S. J. Peale (2010), Analytical model of the long-period forced longitude librations of Mercury, *Icarus*, *207*, 536–544, doi:10.1016/j.icarus.2009.12.020.

Yseboodt, M., A. Rivoldini, T. Van Hoolst, and M. Dumberry (2013), Influence of an inner core on the long-period forced librations of Mercury, *Icarus*, *226*, 41–51, doi:10.1016/j.icarus.2013.05.011.